Progress In Electromagnetics Research B, Vol. 1, 81–94, 2008

ELECTROMAGNETIC MODEL FOR MICROWAVE COMPONENTS OF INTEGRATED CIRCUITS

F. A. Mohammadi

Electrical and Computer Engineering Department
Ryerson University
350 Victoria Street, Toronto, Ontario, M5B 2K3, Canada

M. C. E. Yagoub

School of Information Technology and Engineering
University of Ottawa
161 Louis Pasteur, Ottawa, Ontario, K1N 6N5, Canada

Abstract—This paper presents an accurate and robust time-domain electromagnetic model for microwave components of integrated circuits. The time-domain model has been validated on different structures such as metallic waveguides, planer lines and the transition of waveguide-microstrip line under harmonic oscillation excitation. The results obtained from simulation were compared to the experimental test results. The simulation results demonstrated that the approach is suitable to model microwave components of integrated circuits.

1. INTRODUCTION

The current developments of integrated hybrid and monolithic circuits become crucially important for microwave application. Specifically, in the last few years, the dramatic demand of more and more sophisticated hybrid and monolithic microwave and optoelectronic integrated circuits highlight the crucial need for fast, accurate and robust CAD tools [1, 2]. Due to their complexity, such circuits must be designed using advanced CAD techniques. These techniques must be able to simulate the interaction of electromagnetic (EM) waves with interconnects and passive components where the dimensions become important, and where major difficulties lie. The objective of this paper is to develop a comprehensive, systematic and generic approach

for the global, full-wave simulation of 3D electromagnetic structures. The technique is based on the rigorous solution of Maxwell's equations using explicit finite difference method in time domain (FDTD) [3]. Several absorbing boundary conditions are used to truncate the computational domain [4–7]. This approach has several advantages over any other previous work [8–10]. This approach has been applied to several structures, such as metallic waveguide, planner line [11] to demonstrate its capabilities. The 3D time-domain model is suitable for implementation on Massively Parallel Processing (MPP) machine, and can be used for hybrid and monolithic circuits in microwave as well as optical frequency ranges.

2. ELECTROMAGNETIC MODEL

The EM wave propagation can be completely characterized by solving Maxwell's equations. In natural unity system, assuming uniform, isotropic medium for the dielectric and magnetic relations, Maxwell's equations are given by:

$$\text{Rot } \bar{E} = -\frac{\partial \bar{B}}{\partial t} \qquad \text{Rot } \bar{B} = \frac{c}{\sqrt{\varepsilon_r}}\bar{j} + \frac{\partial \bar{E}}{\partial t}$$

These systems of equations are hyperbolic and symmetric. It can be seen that the dielectric and the permeability (ε, μ) appear only in source terms. This system of equations can be also written:

$$\frac{\partial \bar{U}^t}{\partial t} + A\frac{\partial \bar{U}^t}{\partial x} + B\frac{\partial \bar{U}^t}{\partial y} + C\frac{\partial \bar{U}^t}{\partial z} = \bar{F}$$

where $\bar{U}^t = (E_x,\ E_y,\ E_z,\ B_x,\ B_y,\ B_z)$, $\bar{F} = (-j_x\frac{c}{\sqrt{\varepsilon_r}},\ -j_z\frac{c}{\sqrt{\varepsilon_r}},\ 0,\ 0,\ 0,\ -j_y\frac{c}{\sqrt{\varepsilon_r}})$ and matrix A, B, C are the reel coefficients. c denotes the speed of light. Numerical resolution of Maxwell's equations is based on an explicit finite difference technique where $\bar{E}$ and $\bar{B}$ are unknowns. Mac-Cormack numerical scheme which is a modified Lax-Wendroff scheme have been applied, with two increments in time and in the form of predictor-corrector. Predictor provides an estimate of the solution and corrector decrease the error produced by the predictor and gives a more accurate result.

In this scheme $\bar{E}$ and $\bar{B}$ are calculated at the same point and same time and they are situated at the centre of a space mesh as shown in Fig. 1.

This scheme is adopted to study non-linear hyperbolic systems,

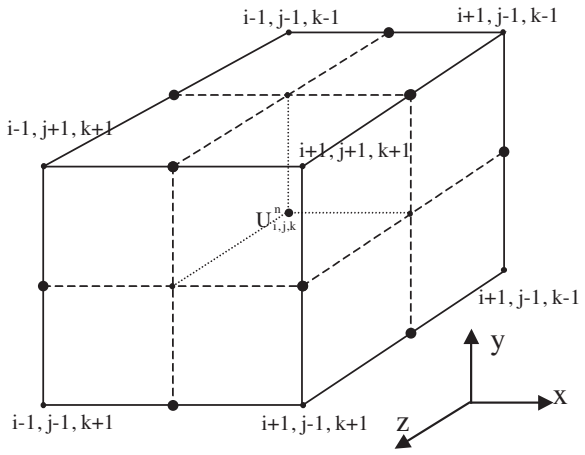

Figure 1. Mac-Cormack's space mesh.

which can be presented in a general form of:

$$\frac{\partial \bar{U}^t}{\partial t} + \frac{\partial \bar{G}}{\partial x} + \frac{\partial \bar{H}}{\partial y} + \frac{\partial \bar{K}}{\partial z} = \bar{F}$$

If Δx, Δy and Δz are defined as space increments and Δt as time increment, the numerical formulation of Maxwell's equations using Mac-Cormack discretization is:

$$\textit{Predictor}: U^{n+\frac{1}{2}}_{i,j,k} = U^n_{i,j,k} - \frac{\Delta t}{\Delta x} A \left(U^n_{i,j,k} - U^n_{i-1,j,k} \right) - \frac{\Delta t}{\Delta y} B \left(U^n_{i,j,k} - U^n_{i,j-1,k} \right) - \frac{\Delta t}{\Delta z} C \left(U^n_{i,j,k} - U^n_{i,j,k-1} \right)$$

$$\textit{Corrector}: U^{n+1}_{i,j,k} = \frac{1}{2} \left(U^n_{i,j,k} + U^{n+\frac{1}{2}}_{i,j,k} \right) - \frac{\Delta t}{2\Delta x} A \left(U^{n+\frac{1}{2}}_{i+1,j,k} - U^{n+\frac{1}{2}}_{i,j,k} \right) - \frac{\Delta t}{2\Delta y} B \left(U^{n+\frac{1}{2}}_{i,j+1,k} - U^{n+\frac{1}{2}}_{i,j,k} \right) - \frac{\Delta t}{2\Delta z} C \left(U^{n+\frac{1}{2}}_{i,j,k+1} - U^{n+\frac{1}{2}}_{i,j,k} \right) + \Delta t \, F^n_{i,j,k}$$

The Mac-Cormack predictor-corrector technique is used in conjunction with the upwind and Lax-Wendroff methods, to achieve stable and accurate solutions. The space increments are adjusted to satisfy wavelength criteria for a stable solution.

The finite difference time-domain technique involves absorbing boundary conditions (ABS's) to truncate the computational domain. The choice of absorbing boundaries is very critical to the overall stability of the finite difference scheme. In a review of some the most common ABC such as, Mur's second order ABC [2], dispersive

boundary condition based on Higdon's ABC and perfectly matched layer (PML) [3, 4] have been implemented in CAD design programs. Choosing the best value for the adjustable parameters in the ABC optimizes Mur's second order ABC. Higdon's boundary conditions are based on the fact that an arbitrary wave can be decomposed into a summation of plane waves with different angles of incidence. It has been observed that the reflections by the Higdon's boundary conditions are an order of magnitude less than those from the first order ABC. Numerical experimentation was performed to obtain the optimum absorption for the given geometry and simulation parameters of the problem.

The modeling tools were combined with a user-friendly shell, resulting in a simulation platform which includes the following options:

- computation of the mutual coupling between the computed modes
- computation of critical design parameters
- volume representations of the field inside the structure (i.e., waveguide) and in the boundary region; the representation include iso-surface and can make use of transparency; the value of the field quantities can be inspected along user-specified surfaces and lines and at user-specified locations.

3. ELECTROMAGNETIC MODELS VERIFICATION

Numerical simulations were performed to demonstrate the capability of the developed modeling tool. Three different structures, metallic waveguide, planner line and under harmonic oscillation excitation were investigated.

3.1. U-Waveguide Simulation

3.1.1. U-Waveguide Structure

The 3D structure used in the simulation of the U-waveguide is shown in Fig. 2(a). The waveguide consists of a rectangular guide and a metallic central conductor with a length of w, called U or ridge, and a locally decreasing gap of h between ridge and internal boundary of guide (Fig. 2(b)).

This gap changes linearly as a function of abscise Oz.

This structure can be excited by electromagnetic wave in TE_{10} mode on the input plan of the waveguide (Fig. 2(a)). It can be shown that under these conditions the structure act like an impedance transformer between input plan and output plan of the waveguide.

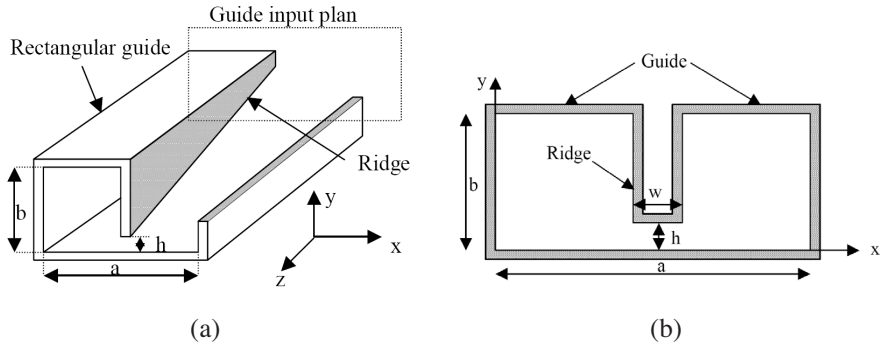

Figure 2. (a) U-waveguide (b) U-waveguide in vertical plan.

The U-waveguide was modeled using parallelepipeds elements. The ridge has been meshed in yz plan by a series of steps as shown in Fig. 3.

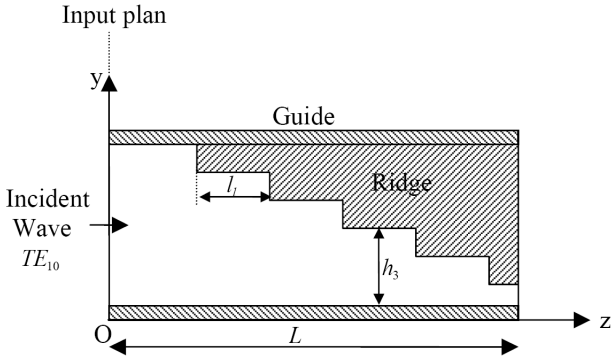

Figure 3. U guide input plan.

These steps have different lengths. The differences are a multiple of quarter wavelength ($\lambda_g/4$), to prevent the resonance phenomena (cavities). The heights of these steps have been chosen so as to minimize the electromagnetic wave reflection. Finally the waveguide length L, (see Fig. 3) has a value of $3\lambda_g/2$ at 100 GHz frequency. The space increments were adjusted to satisfy wavelength criteria for a stable solution.

3.1.2. Harmonic Oscillation Analysis

The simulation parameters of U-waveguide are listed in Table 1. These parameters are in the range of the mm-wave length.

Table 1. U-Waveguide characteristics.

Frequency band (GHz)	75−110
Waveguide width a (mm)	2.54
Waveguide height b (mm)	1.27
Waveguide length L (mm)	9.024
Analysis frequency (GHz)	100
Ridge height h (μm)	127
Ridge width w (μm)	Variable (Based on the choice of the characteristic impedance)

A TE_{10} electromagnetic field was applied at the input plan of waveguide as shown in Fig. 3. The TE_{10} electromagnetic field has the following expression:

$$\begin{aligned} E_{y_i} &= E_{yo} \sin \frac{\pi x}{a} \cos 2\pi.F.t \\ B_{x_i} &= B_{xo} \sin \frac{\pi x}{a} \cos 2\pi.F.t \\ E_{x_i} &= E_{z_i} = B_{y_i} = B_{z_i} = 0 \end{aligned}$$

A $40 \times 40 \times 80$ mesh that covers the 3D structure was used. The time necessary to obtain a steady state was about ten times the period of the input signal. Sampling rate was ten ps.

Energy confinement effect of electromagnetic wave under the ridge can be observed in Fig. 4(a). This figure shows the evolution of the S_x component of the Poynting vector. The power density distribution in the xy plan of waveguide is illustrated in Fig. 4(b). The clearest zone indicates where power density is maximum. In this case it is located under the ridge.

Figure 5 depicts 3D electrical field (E_x) and magnetic induction (B_y) evolution at different points. The effect of discontinuity induce by the ridge on EM fields is well illustrated in this figure.

3.2. Planner Lines Simulation

3.2.1. Harmonic Oscillation Analysis of a Microstrip Line

The simulation parameters of the microstrip are $h = 190\,\mu$m, $\varepsilon_r = 2.2$ and $W = 380\,\mu$m as shown in Fig. 6. A $70 \times 40 \times 130$ mesh that covers the 3D structure was used. The width of metallic strip (W) and the

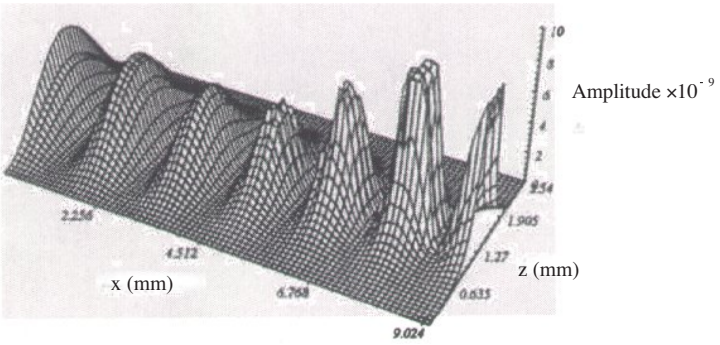

(a)

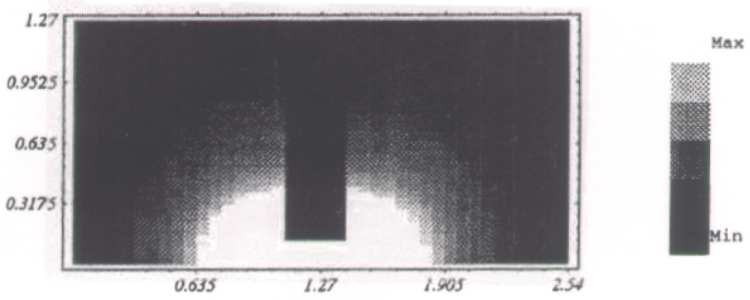

(b)

Figure 4. (a) $S_Z(x, z)$ Poynting vector (b) Flux of Poynting vector $S_Z(x, z)$ in a vertical plan.

thickness of dielectric substrate (h) are divided respectively to six and four meshes.

The length L_z of the microstrip is about 12 mm which is three times the guided wave length in dielectric for an input signal at 60 GHz. The microstrip has been excited at the input plan by the electromagnetic field with the following components:

$$E_y = E_{yo} \cos 2\pi.F.t \qquad B_x = B_{xo} \cos 2\pi.F.t$$

This electromagnetic field is applied all along the dielectric substrate thickness and metallic strip length (Fig. 6). At the remaining part of the input plan, the boundary conditions which represent the electrical short circuit have been applied. This type of excitation always creates discontinuity at the input plan. The evolution of Poynting vector shows (Fig. 7(a)) that the dominated

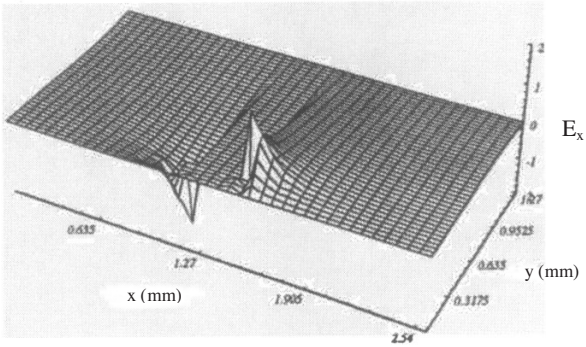

(a)

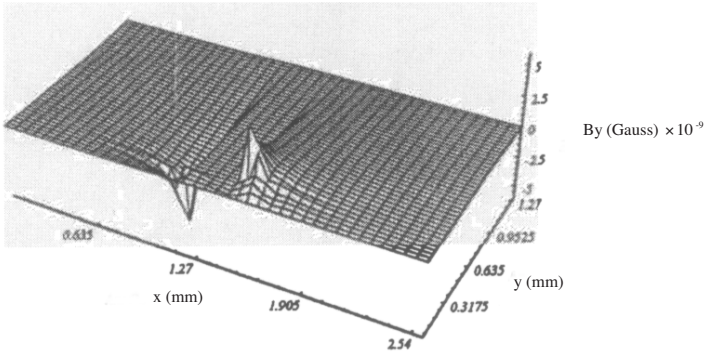

(b)

Figure 5. (a) $E_x(x, y)$ Electrical Field (b) $B_y(x, y)$ Magnetic induction in a vertical plan of U-waveguide.

mode propagation direction. This is because the microstrip is not long enough to permit the establishment of the quasi TEM mode. Given the initial excitation applied to the microstrip, the presence of the higher order mode which is due to microstrip line scattering is illustrated in Fig. 7(b).

The effect of the scattering [12] and confinement of the electromagnetic energy by microstrip line are shown in Fig. 8. This figure shows the Poynting vector flux in two different sections of xy plan at about 4 mm (Fig. 8(a)) and at 9 mm (Fig. 8(b)) from the input plan.

The importance of the line scattering can be seen in Fig. 8(a). This is due to the fact that quasi TEM mode is not yet established. On the contrary, Fig. 8(b) shows that a big part of the electromagnetic energy

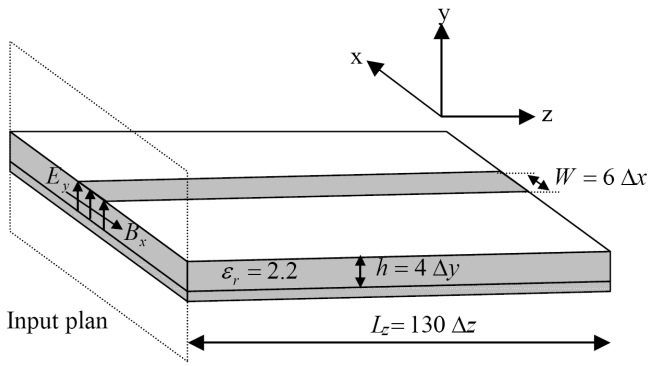

Figure 6. Microstrip line.

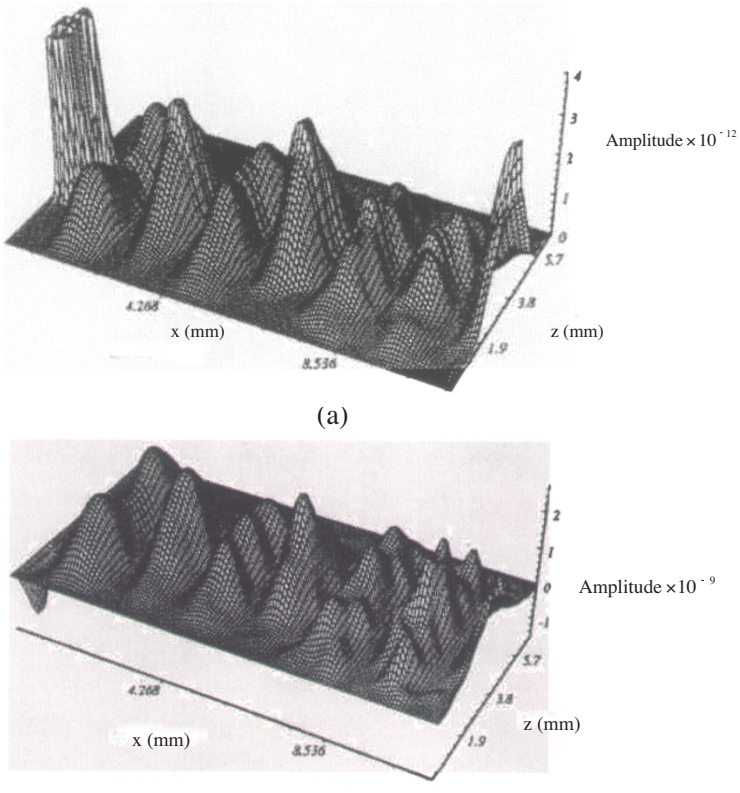

Figure 7. $S_z(x, z)$ Poynting vector (a) in dielectric substrate (b) in the air.

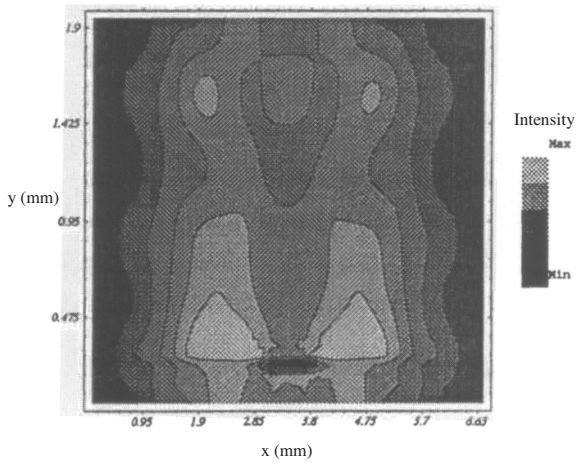

(a)

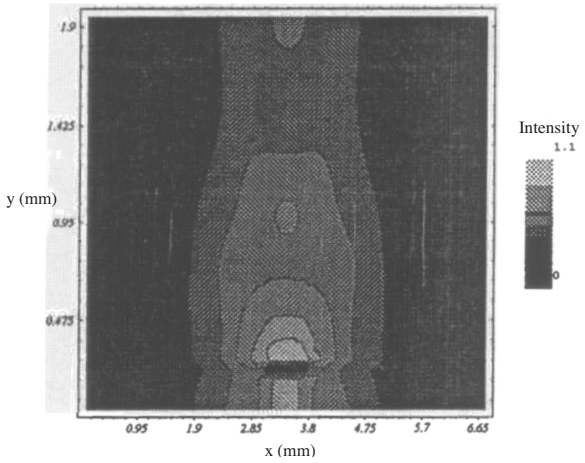

(b)

Figure 8. Flux of Poynting vector (a) at 4 mm (b) at 9 mm from the source plan.

is confined under the metallic strip due to progressive establishment of the quasi TEM propagation. However, the presence of scattering wave by the metallic strip which is due to scattering in the air section of the microstrip line can be seen.

3.3. Transition of Waveguide-Microstrip Line

The topology of the transition between waveguide-microstrip was illustrated in Fig. 9. The U guide has the geometric characteristics expressed at Section 3.1. These characteristic have been used both in simulation efforts and during experimental test program. In addition, the structure and properties of the microstrip line is similar to one described at Section 3.2. However the length of microstrip line is limited to 4 mm.

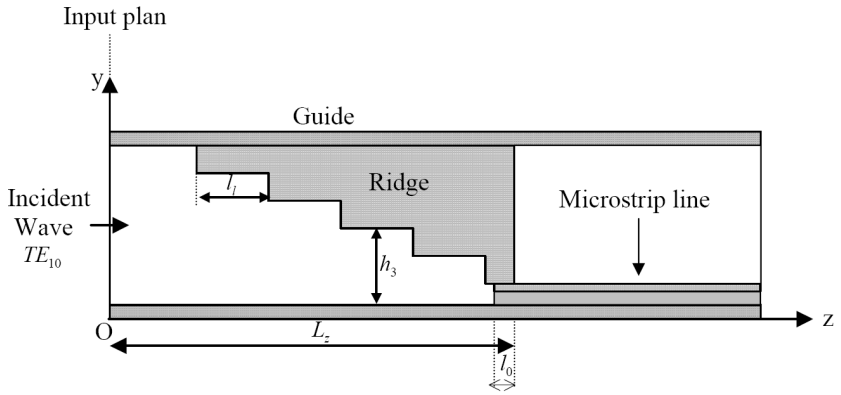

Figure 9. Topology of the transition between Waveguide and microstrip line.

Simulation and experimental test conditions are as follow:

- To simulate the transition part, the line is inserted with a length and height similar to rectangular guide (Fig. 9), the non-reflecting boundary conditions are applied at the exterior boundary of microstrip line which describes a perfect impedance adaptation.
- In experimental part, A 50 Ω impedance is applied on substrate of the microstrip line. The measurement of experimental characteristic has been performed using a characteristic impedance network analyzer.

Our methodology was to obtain the best adaptation impedance between the waveguide and microstrip line based on predefined geometric characteristics. To achieve this, the evolution of the impedance characteristic, Zc, of waveguide and microstrip line as a function of the geometrical parameters of the guide at 60 GHz was shown in Fig. 10. This figure shows that impedance adaptation criteria at 50 Ω give a ridge width of 680 μm and a line width of 380 μm. However under these conditions, the ridge is much larger than the

microstrip line, therefore, non-adaptation of transition occurs. In fact, electromagnetic field in a vertical section of ridge (Fig. 5) indicated that electromagnetic energy was uniformly localized under the ridge. Consequently, if the microstrip line length is much smaller than the ridge, a part of energy will not be coupled with the microstrip line and will reflect toward the waveguide. Therefore, an identical microstrip line and ridge length of 400 μm has been chosen.

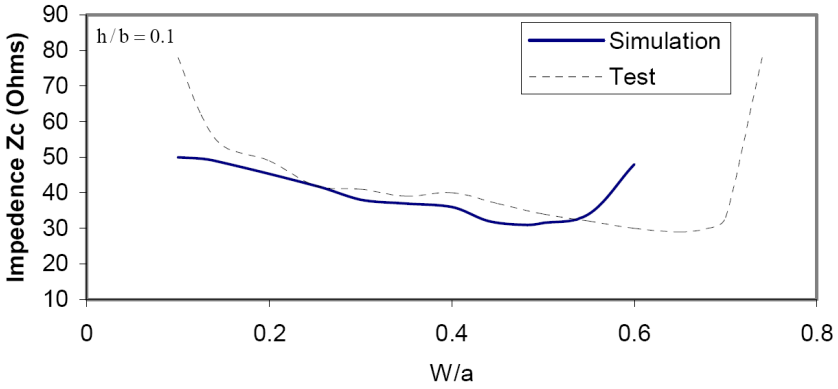

Figure 10. Topology of the transition between waveguide and microstrip line.

The experimental test results of the reflection coefficient measured at 60 GHz were compared to the results obtained from simulation as shown in Fig. 11. The evolutions of both measured and simulated reflection coefficient are shown versus penetrated length of microstrip line under the ridge. The reading of the (l_0) position performed with variable thickness from 7 to 8 mm and a space increment of 100 μm. The optimal l_0 penetrated length of microstrip line shows a good agreement between the simulation results and the experimental test results. The differences between experimental test and simulation results were not great. The small difference between simulation estimates and test data can be explained by imprecision of measurement of the thickness after settling. However, the minimum value of S11 coefficient, obtained from simulation, is more conservative than the measured one. The small difference between simulation estimates and test data is contributed to 50 Ω charge imperfection which connected to the microstrip line.

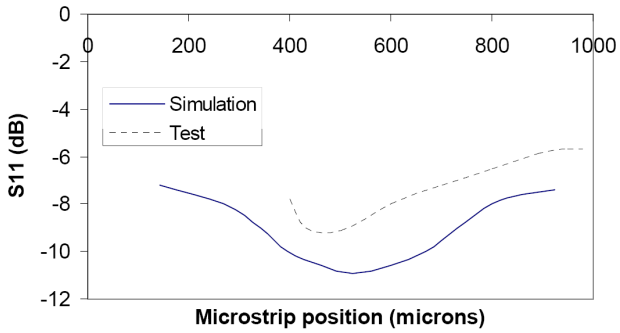

Figure 11. Simulated and experimental reflection coefficient (S11).

4. CONCLUSION

A robust and accurate 3D-EM model using the FDTD technique has been developed to simulate microwave structures. This model has been successfully demonstrated through the simulation of metallic waveguides, planar lines and waveguide-microstrip line transition for harmonic oscillation analysis. The obtained results were in good agreement with experimental results obtained from characterization of a waveguide-microstrip line transition at 60 GHz. The approach is suitable to model microwave components and high speed interconnects of integrated circuits. Evaluation of the model showed that it is computationally stable, reliable and repeatable.

ACKNOWLEDGMENT

The authors wish to acknowledge the supports provided by Ryerson University.

REFERENCES

1. Park, J. K., D. H. Shin, J. N. Lee, and H. J. Eom, "A full-wave analysis of a coaxial waveguide slot bridge using the Fourier transform technique," *J. Electromagnetic Waves Application*, Vol. 20, No. 2, 143–158, 2006.
2. Tan, K.-B., L. Li, and C.-H. Liang, "Canonical analysis for dissipative electromagnetic medium," *J. Electromagnetic Waves Application*, Vol. 21, No. 11, 1499–1505, 2006.

3. Taflove, M. A., *Computational Electrodynamics: The Finite-Difference Time-Domain Method*, 2nd edition, Artech House, Norwood, MA, 2000.
4. Mur, G., "Total field absorbing boundary conditions for the time domain electromagnetic field equations," *IEEE Trans. on Electromagnetic Compatibility*, Vol. 40, No. 2, 100–102, May 1998.
5. Berenger, J. P., "Making use of the PML absorbing boundary condition in coupling and scattering FDTD computer codes," *IEEE Trans. on Electromagnetic Compatibility*, Vol. 45, No. 2, 189–197, May 2003.
6. Yu, T.-B., B.-H. Zhou, and B. Chen, "An unsplit formulation of the Berenger's PML absorbing boundary condition for FDTD meshes," *IEEE Microwave and Wireless Components Letters*, Vol. 13, Issue 8, 348–350, Aug. 2003.
7. Watanabe, K. and K. Yasumoto, "Two-dimensional electromagnetic scattering of non-plane incident waves by periodic structures," *Progress In Electromagnetics Research*, PIER 74, 241–271, 2007.
8. Gedney, S. D., G. Liu, J. A. Roden, and A. Zhu, "Perfectly matched layer media with CFS for an unconditionally stable ADI-FDTD method," *IEEE Trans.on Antennas and Propagation*, Vol. 49, 1554–1559, Nov. 2001.
9. Arndt, F., R. Lotez, and J. Ritter, "Advanced FD-TD techniques for the CAD of microwave components," *Electromagnetics*, Vol. 23, 153–168, Feb.–Mar. 2003.
10. Jiao, D. and J. M. Jin, "Time-domain finite-element modeling of dispersive media," *IEEE Trans. Microwave and Wireless Components Letters*, Vol. 11, 220–223, May 2001.
11. Arnold, M. D., "An efficient solution for scattering by a perfectly conducting strip grating," *J. Electromagnetic Waves Application*, Vol. 20, No. 7, 891–900, 2006.
12. Gelius, L.-J., "Electromagnetic scattering approximations revisited," *Progress In Electromagnetics Research*, PIER 76, 75–94, 2007.